Received 3 January 2021; revised 7 February 2021; accepted 8 February 2021. Date of publication 17 February 2021; date of current version 9 March 2021.

Digital Object Identifier 10.1109/OJAP.2021.3059468

Profile Inversion and Closed Form Formulation of Compact GRIN Lenses

FRANCESCA MAGGIORELLI[1], ANASTASIOS PARASKEVOPOULOS[1], J. C. VARDAXOGLOU[1,2] (Fellow, IEEE), MATTEO ALBANI[1] (Fellow, IEEE), AND STEFANO MACI[1] (Fellow, IEEE)

[1]Department of Information Engineering and Mathematics, University of Siena, 53100 Siena, Italy

[2]School of Mechanical, Electrical, and Manufacturing Engineering, Loughborough University, Loughborough LE11 3TU, U.K.

CORRESPONDING AUTHOR: F. MAGGIORELLI (e-mail: francesca.maggiorelli@unisi.it)

This work was supported by Huawei Technologies Company Ltd., within the joint Innovation Antenna Lab between Huawei and the Department of Information Engineering and Mathematics, University of Siena.

ABSTRACT New formulas for the design of cylindrical Graded-Index (GRIN) lens-antennas with integrated feeder are presented. The possibility of integrating the feeder within the lens makes the system more compact, avoids complex mechanical design and alignment errors. The lens is characterized in analytical form by Geometrical Optics (GO). The expression of the radially varying refractive index is derived by applying the conservation of the momentum inside the lens and imposing parallel rays at the lens output interface. The mathematical procedure to retrieve the refractive index is based on the inversion of a truncated Abel transform. The Poynting vector at the lens aperture is derived by applying the conservation of energy in each elementary ray-tube. By approximating the Poynting vector to a Gaussian function the total efficiency of the lens-antenna is derived in a closed form, allowing for a quick lens design. The proposed formulation has been successfully validated by using ray-tracing and a full-wave simulations. Finally, we present examples of practical design of GRIN lenses by using holes of different shapes in a dielectric ABS/Teflon host media.

INDEX TERMS Lens-antennas, dielectric lenses, inhomogeneous lenses.

I. INTRODUCTION

GRADED Index (GRIN) lenses are popular due to their focusing properties and their application as high gain antennas. Several GRIN lens configurations have been reported in the literature, including the well-known Luneburg [1] and half-Maxwell fisheye [2]. The design usually provides the transformation of a spherical wave into a plane wave, resulting in a highly directive beam. The limitation of these lenses is related to their bulky size and weight in the 3D configuration. In microwaves, they are difficult to be manufactured with conventional methods. With the advent of the 3D printing technology, they can be easily manufactured by varying the material density. Moreover, the installation and alignment become a demanding process. A GRIN lens with an integrated feeder overcomes the above difficulties and it is proposed in this paper. To solve such limitations GRIN lens with an integrated feeder has been studied in this paper.

An interesting approach to design GRIN lenses is to employ Transformation Optics (TO) [3]–[9] or quasi-TO [10]. Through a coordinate transformation TO manages to reshape the lens profile to realize a flat GRIN lens with low aberrations, and convenient integration with planar feeder. However, the achieved shape and design parameters are applicable only in a narrow frequency range and requires anisotropic permittivity and permeability values, which are almost impossible to be realized in practice with a good accuracy. Therefore, approximations need to be made on the final TO solution that significantly deteriorate the antenna performance, which results to be inferior to the one designed by Geometrical Optics (GO) ray-solution [11], [12]. Although GO loses some validity

around caustics (where it becomes singular) and around shadow boundaries (where it has to be complemented by diffracted rays), in focusing media it leads to a convenient approximation of the aperture field and subsequently one can use Physical Optics (PO) for the far field prediction. The aperture field can be estimated through tracing of the curvilinear GO rays; these rays are locally orthogonal to the wave fronts of the propagating field in isotropic GRIN media. While the ray tracing gives the phase of the aperture field, the amplitude can be evaluated by applying the energy transport equation, which expresses the conservation of the energy in each elementary ray-tube [13], [14]. Unfortunately, the GRIN profile realizing focusing condition requires the solution of a non-linear integral equation, which is rarely obtained in an analytical form.

In this paper, we derive the exact solution for a radial refractive index profile of a GRIN lens with integrated feeder, namely a GRIN lens with a zero focal-length. Assuming that the focus is inside the medium, the radially varying refractive index profile is derived in analytical form via the inverse truncated Abel transform. This differs from the conventional Abel transform since a finite limit integration is used to define the transform. Although the GRIN solution for infinite cylinder and radial graded index exists in the literature, it is mostly used in the framework of fiber optics [15], [16]. The application to antennas has not been investigated for this zero focal-length lens, in contrast with the more popular GRIN lens with non-zero focal length (without an integrated feeder) [17]–[20]. To the authors knowledge the above integration with a clear explanation and the analytical derivation for solving the non-linear integral equation required to describe the problem cannot be found in the literature. Therefore, additional information is presented here to render this derivation complete.

Based on ray-paths and of the refractive index profile, we derive here the Poynting's vector at the lens aperture by applying the conservation of energy in elementary ray-tubes. Upon choosing the parametric $\cos^m\theta$ varying function to approximate the feed intensity pattern, we found that the achieved power density of the aperture could be conveniently approximated by a Gaussian distribution. Thus, allowing for a closed form expression for tapering and spill-over efficiency to be derived in a closed analytical form. The closed form expression of the total efficiency gives the possibility of designing the system in a straightforward quick way avoiding optimization processes [21]. The formulation presented here is validated with a ray-tracing algorithm, solving numerically for the ray-paths and Poynting's vector at the aperture, as well as with results from a full wave analysis.

The article is organized as follows. Section II presents the GO analytical solution of the GRIN lens refractive index and of the ray-paths inside the lens. Section III provides a closed form expression for the power density and its Gaussian approximation as well as a closed form expression for the aperture efficiency. Section IV provides a numerical validation for that formula by ray tracing and full-wave analysis. Section V shows an example of GRIN implementation through a homogenized medium constituted by holes in a host dielectric fed by an integrated waveguide. Section VI draws the conclusions.

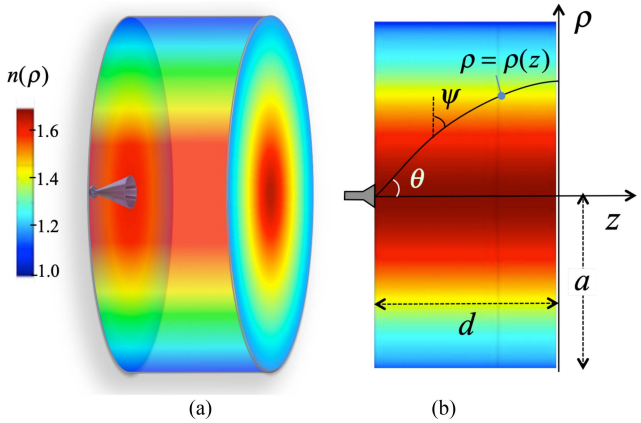

FIGURE 1. Flat inhomogeneous GRIN lens and coordinate systems. (a) 3D view. (b) 2D view; the black curved line represents the ray-path of a ray launched with an angle θ from the focus.

II. DIRECT INVERSION AND RAY-PATHS

Let us consider a flat inhomogeneous circular symmetric lens with refractive index $n(\rho)$. Rays are launched with different angles θ from a point source positioned at the center of the lens input interface.

From the point source the rays propagate inside the lens by following curvilinear ray-path because of the radial dependency of the refractive index of the medium. Each trajectory forms an angle ψ between the radial direction ρ and the local ray direction. The conservation of the wavenumber component along the direction z (also known in optics as conservation of the momentum) can be written as $L = n(\rho)\sin\psi(\rho) = n_0\cos\theta$ along the ray trajectory, where n_0 is the maximum GRIN value assumed to be on the axis. The latter can be rearranged as $\tan\psi = L/(n\sqrt{1-(L/n)^2}) = n_0\cos\theta/\sqrt{n^2-n_0^2\cos^2\theta}$.

The ray-path can be obtained in the form $z = z(\rho)$ by integrating along ρ its derivative $dz/d\rho = \tan\psi$, thus providing

$$z(\rho) = \int_0^{\rho} \frac{n_0\cos\theta}{\sqrt{n(\rho')^2 - n_0^2\cos^2\theta}} d\rho' \tag{1}$$

The rays reach the maximum of their trajectory ρ_{out} when $\psi = \pi/2$ and $L = n_0\cos\theta = n(\rho_{out})$. The point in which this occurs is denoted by turning point. The focusing condition occurs at those value of thickness d for which the condition $L = n(\rho_{out})$ is satisfied for all the rays, namely all the rays arrive at their turning point independently on their initial momentum. This leads to

$$d = \int_0^{\rho_{out}} \frac{n(\rho_{out})}{\sqrt{n(\rho)^2 - n^2(\rho_{out})}} d\rho, \quad n(\rho_{out}) = n_0\cos\theta \tag{2}$$

A. DIRECT INVERSION OF THE INDEX PROFILE

The solution of the integral equation (2) is known in optics since it is used in graded index optical fibers [15]. However, the procedure of the solution, is not well known; therefore, it is appropriate to derive it by resorting to the inverse 'truncated' Abel transform as described below. First, we normalize the refractive index and the momentum by n_0, thus obtaining

$$d = \int_0^{\rho_{\max}} \frac{l}{\sqrt{\eta^2(\rho) - l^2}} d\rho \tag{3}$$

where $l = \cos\theta$, $\eta = n/n_0$. The ray path equation is first manipulated by using the change of variable $\eta = \eta(\rho)$ and therefore $\rho = \rho(\eta)$. We can hence write (3) as:

$$d = -\int_l^1 \frac{d\rho}{d\eta} \frac{l}{\sqrt{\eta^2 - l^2}} d\eta \tag{4}$$

In (4) the unknown function becomes $\rho = \rho(\eta)$ which is the inverse function of $\eta = \eta(\rho)$. Eq. (4) can be thought of as the inverse truncated Abel transform of the function $\rho = \rho(\eta)$. Indeed the Abel transform and inverse transform for a couple of functions $f(l)$ and $F(\eta)$ with variables l and η can be written as:

$$f(l) = -\frac{1}{2\pi} \int_l^\infty \frac{dF(\eta)}{d\eta} \frac{1}{\sqrt{\eta^2 - l^2}} d\eta \tag{5}$$

$$F(\eta) = \int_\eta^\infty \frac{f(l) l}{\sqrt{l^2 - \eta^2}} dl \tag{6}$$

in which the upper limit is infinity. On the other hand, in (4) the upper limit is 1, and this requires the introduction of a "truncated" version of the Abel transform which complicates the inverse-type relationship. To proceed with a direct inversion, the steps below may be followed

i) change formally l into l' and η into η' in (4),
ii) multiply both members of it by $1/\sqrt{l'^2 - \eta^2}$,
iii) integrate both members in dl' from η to 1

With these steps we obtain:

$$\int_\eta^1 \frac{d}{\sqrt{l'^2 - \eta^2}} dl' = -\int_\eta^1 \left[\int_{l'}^1 \frac{d\rho}{d\eta'} \frac{l'}{\sqrt{\eta'^2 - l'^2}} d\eta' \right] \times \frac{1}{\sqrt{l'^2 - \eta^2}} dl' \tag{7}$$

Next, the order of integration is interchanged by applying Fubini's theorem (note that on the integration region the argument inside the square-roots remain non-negative), thus leading to:

$$\int_\eta^1 \frac{d}{\sqrt{l'^2 - \eta^2}} dl' = -\int_\eta^1 \frac{d\rho}{d\eta'} \times \left[\int_\eta^{\eta'} \frac{l'}{\sqrt{l'^2 - \eta^2}\sqrt{\eta'^2 - l'^2}} dl' \right] d\eta' \tag{8}$$

By recognizing that:

$$\frac{l'}{\sqrt{l'^2 - \eta^2}\sqrt{\eta'^2 - l'^2}} = \frac{d}{dl'} \arcsin\left(\frac{\sqrt{l'^2 - \eta^2}}{\sqrt{\eta'^2 - \eta^2}} \right) \tag{9}$$

and by inserting (9) in (8), leads to:

$$\begin{aligned} \int_\eta^1 \frac{d}{\sqrt{l'^2 - \eta^2}} dl' &= -\int_\eta^1 \frac{d\rho}{d\eta'} \left[\arcsin\left(\frac{\sqrt{l'^2 - \eta^2}}{\sqrt{\eta'^2 - \eta^2}} \right) \right]_\eta^{\eta'} d\eta' \\ &= -\int_\eta^1 \frac{d\rho}{d\eta'} \frac{\pi}{2} d\eta' = -\frac{\pi}{2} \int_\rho^0 d\rho = \frac{\pi}{2} \rho \end{aligned} \tag{10}$$

which can be rearranged as

$$\rho(\eta) = \frac{2}{\pi} \int_\eta^1 \frac{d}{\sqrt{l^2 - \eta^2}} dl. \tag{11}$$

Eq. (11), together with (4), generalizes the Abel transform and inverse transform to the case of unity upper endpoint, i.e., to the case of a truncated Abel transform. Therefore, the solution of (11) can be obtained as the inverse truncated Abel transform of a constant function $d(l) = d$. To this end, the use of the identity

$$\int_\eta^1 \frac{1}{\sqrt{l^2 - \eta^2}} dl = \ln\left(\frac{1 + \sqrt{1 - \eta^2}}{\eta} \right) = \operatorname{arccos} h\left(\frac{1}{\eta} \right), \tag{12}$$

leads to

$$\rho(\eta) = \frac{2d}{\pi} \operatorname{arccos} h\left(\frac{1}{\eta} \right) \tag{13}$$

which is finally inverted leading to

$$n(\rho) = n_0 / \cosh\left(\frac{\pi}{2d} \rho \right). \tag{14}$$

By assuming a lens of radius a and characterized by a continuous refractive index distribution such as its value at the lens side edges matches the free-space refractive index, we obtain:

$$n_0 = \cosh\left(\frac{\pi a}{2d} \right); \quad \frac{d}{a} = \frac{\pi}{2} \frac{1}{\cosh^{-1} n_0} \tag{15}$$

The refractive index as a function of ρ is given in Fig. 2. It is seen that the value of the maximum refractive index becomes rapidly large for decreasing values of $d/(2a)$. These large values cannot be applied in practice since the discontinuity at the output interface would create reflections, therefore, limiting the practical applicability to very thick lenses, unless a terminal matching layer is used. This aspect will be quantified in Section III-C.

Before proceeding further, we should stress the fact that a closed form expression of the refractive graded index for focusing lenses cannot be obtained in a closed analytical form except for few cases. The one obtained here is one of this few cases

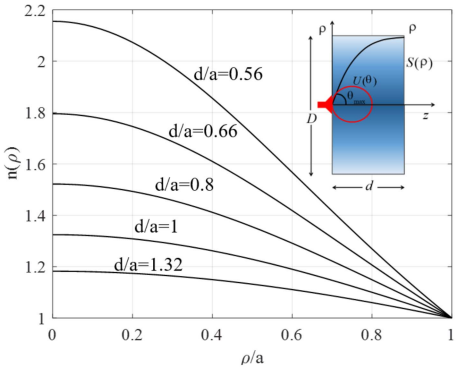

FIGURE 2. Refractive index distribution for different values of the ratio *d/a*, where *d* is the lens thickness and *a* is the lens radius.

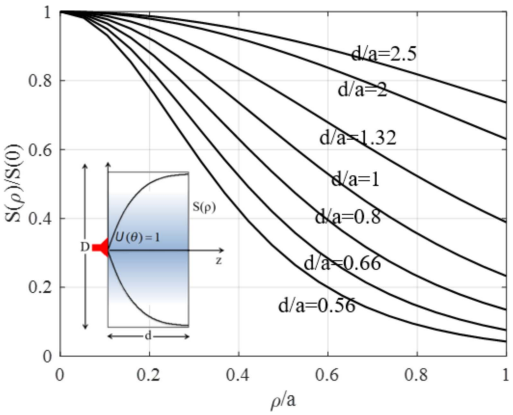

FIGURE 3. Distribution of normalized power density on the aperture with respect to the normalized radius for various values of the ratio *d/a*.

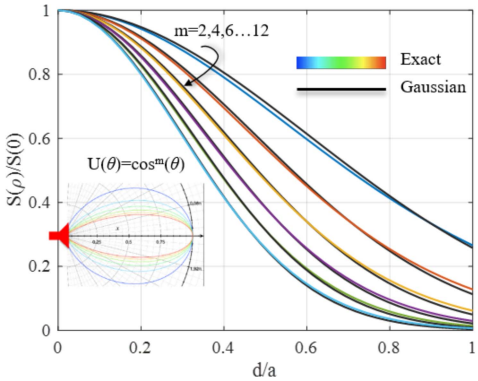

FIGURE 4. Power density on the aperture obtained by $U(\theta) = \cos^m \theta$ feed; GO solution (colored lines) and Gaussian approximation (black lines) for *m* ranging from 2 to 12.

B. CLOSED FORM EXPRESSION OF THE RAY-PATH

Inserting (14) in (1) and making the substitution $x = \cosh(\gamma\rho)$ with $\gamma = \pi/2d$, gives the integral form for the ray-paths $z = \gamma^{-1}\int_1^{\cosh(\gamma\rho)}(\tan^2\theta - x^2)^{-1/2}dx$ which can be solved in exact form as [23, p. 86],

$$z = \frac{1}{\gamma}\arcsin\left[\sinh(\gamma\rho)\cot\theta\right] \tag{16}$$

which inverted leads to

$$\rho = \frac{1}{\gamma}\sinh^{-1}\left[\tan\theta\sin(\gamma z)\right] \tag{17}$$

The latter is the explicit expression of the ray-paths for any ray starting with an arbitrary angle θ.

III. POWER DENSITY AND APERTURE EFFICIENCY

A. POWER DENSITY AT THE LENS INTERFACE

The incident Poynting vector $S(\rho)$ at the output interface $z = d$ is obtained by the conservation of energy in each elementary ray-tube from the feed. Denoting by $U(\theta)$ the radiation intensity of the feed, the power flowing in an elementary ray-tube of solid angle $\sin\theta d\theta d\varphi$ is given by $U(\theta)\sin\theta d\theta d\varphi$; this power is preserved along the ray till the aperture, where it can be expressed as $S(\rho)d\rho d\varphi$. Equating the two expressions leads to

$$S(\rho) = U(\theta)\frac{\sin\theta}{\rho}\frac{d\theta}{d\rho} \tag{18}$$

Substituting z = d in (17) and using (15) leads to

$$\rho = \frac{2d}{\pi}\sinh^{-1}[\tan\theta];\ \ \theta = \tan^{-1}\left(\sinh\left(\frac{\pi\rho}{2d}\right)\right) \tag{19}$$

which, after some algebraic steps, gives

$$\frac{S(\rho)}{S(0)} = U(\tan^{-1}(\sinh(y)))\frac{\tanh(y)}{y\cosh(y)} \tag{20}$$

where $y = \pi\rho/2d$. We notice that the distribution only depends on d which is linked to the maximum value n_0 through (14). The distribution of normalized power is given in Fig. 3 for an isotropic source ($\underline{U}(\theta) = 1$).

It should be practically convenient to use parametric feed patterns as a reference for the evaluation of the lens design. To this end we adopt the feed type used in [22, p. 813], with radiation intensity given by:

$$U(\theta) = \cos^m\theta \tag{21}$$

These feeds have a gain of $2(m+1)$ and produce, for a given value of n_0, a normalized power distribution

$$\frac{S(\rho)}{S_0} = \frac{\tanh(y)\cos^m\left(\tan^{-1}(\sinh(y))\right.}{x\cosh(y)}\ \ m = 2, 4, \ldots;$$
$$y = \frac{\rho}{a}\cosh^{-1}n_0 \tag{22}$$

which is obtained by substituting eq. (21) in (20). The obtained profiles can be approximated by

$$\frac{S(\rho)}{S_0} = \exp\left(-(0.5m + 0.65)\left(\frac{\rho}{a}\cosh^{-1}n_0\right)^2\right) \tag{23}$$

which is valid for $n_0 \in [1.2, 2]$, $(d/a \in [1.2, 2.5])$, with maximum error less that 3% for m ranging from 2 up to 12.

Fig. 4 presents the Gaussian closed form approximation (black curves) against the exact solution of the normalized power for $n_0 = 1.44$ (Teflon) with m spanning from 2 to 12 with even values.

B. EFFECT OF REFLECTIONS AT THE OUTPUT INTERFACE

Fig. 2 shows that, in order to satisfy the focusing conditions while reducing the thickness d, the dielectric constant has to be increased. However, increasing the dielectric constant entails the risk to have power reflected back from the lens output interface. This implies feed mismatch and even a distortion of the aperture power density with respect to the optimal one. An estimate of the aperture power density $S_{out}(\rho)$ at the output interface is obtained by accounting for reflections through a local non-dispersive transmission line equivalent model.

$$S_{out}(\rho) = S(\rho)T(\rho), T(\rho) = \left\{1 - \left[\frac{n(\rho)-1}{n(\rho)+1}\right]^2\right\} \quad (24)$$

In (24), T(ρ) is the local transmission coefficient expressed as $1 - \mathrm{R}(\rho)$, where R(ρ) is the local reflection coefficient.

C. APERTURE EFFICIENCIES FOR STANDARD FEED PATTERN

It is worth to point out that the presented lens can be used as a Gaussian aperture antenna, as discussed in Section III-A. Such a feature is particularly relevant for reflector antenna applications, where Gaussian feeding is often desired. In this context, it is convenient to analytically predict the gain of the lens, which can be written as

$$G = (ka)^2 \varepsilon_{tap}\varepsilon_{spill}\varepsilon_{tran} \quad (25)$$

where $\varepsilon_{tap}, \varepsilon_{spill}, \varepsilon_{trans}$ denote the tapering, spill-over and transmission efficiencies, respectively. The tapering efficiency is defined here as the ratio between the maximum power intensity in the far region and the power captured by the aperture. In GO assumption, this leads to eq. (26). The spill-over efficiency is the ratio between the total power radiated by the feed (namely transported by all launched rays) and the power arriving to the aperture (namely transported by those rays captured by the aperture, see Fig. 6). Neglecting the contributions of diffracted rays, this leads to eq. (27). The transmission efficiency is indeed the ratio between the power transmitted through the aperture and the one incident (eq. 28).

$$\varepsilon_{tap} = \frac{2\left|\int_0^a \sqrt{S(\rho)}\rho d\rho\right|^2}{a^2 \int_0^a S(\rho)\rho d\rho} \quad (26)$$

$$\varepsilon_{spill} = \frac{\int_0^{\theta_{\max}} U(\theta)\sin\theta d\theta}{\int_0^{\pi} U(\theta)\sin\theta d\theta} \quad (27)$$

$$\varepsilon_{trans} = \frac{\left|\int_0^a \sqrt{T(\rho)S(\rho)}\rho d\rho\right|^2}{\left|\int_0^a \sqrt{S(\rho)}\rho d\rho\right|^2} \quad (28)$$

In (27) $\theta_{\max}$ is the maximum angle for which the ray is captured by the output aperture and $T(\rho)$ is defined in (24). Substituting $\rho = a$ in (19), one has

$$\theta_{\max} = \tan^{-1}\left[\sinh\left(\frac{\pi a}{2d}\right)\right] = \tan^{-1}\left[\sqrt{n_0^2 - 1}\right] \quad (29)$$

It is observed that for $n_0^2 = 2$, $\theta_{\max} = 45°$. We also note that $\varepsilon_{tap}, \varepsilon_{spill}, \varepsilon_{trans}$ do not depend on the frequency under the GO assumption, and their values can be universally depicted as a function of d/a independently of the lens radius electrical size (i.e., a in terms of the wavelength).

Using (23) in (26) and (21) in (27) leads to the closed form expressions

$$\varepsilon_{tap} = \frac{4}{\delta}\tanh\left(\frac{\delta}{4}\right); \delta = (0.5m + 0.65)\left(\frac{a\pi}{2d}\right)^2 \quad (30)$$

$$\varepsilon_{spill} = 1 - \cos^{m+1}\left[\tan^{-1}\left(\sinh\left(\frac{\pi a}{2d}\right)\right)\right] \quad (31)$$

which can be rephrased in terms of n_0 through (14). The above expression can be extended to a generic feed with gain G_f setting $G_f = 2(m+1)$, namely $m = \frac{1}{2}G_f - 1$. Note that The Gaussian approximation of the Poynting vector has been used in the evaluation of the tapering efficiency in (31).

Fig. 5 shows the individual contributions (Fig. 5 a-c) to the total aperture efficiency (Fig. 5 d) as a function of d/a for different exponent in $U(\theta) = \cos^m\theta$ feed pattern. As expected, the total efficiency exhibits a maximum for different values of d/a (and therefore n_0). This gives a convenient way to design the optimal lens for any thickness. For any values of m, the maximum possible efficiency is always between 70% and 80%. Suggested values are $n_0 = 1.44$, $d = 1.73a$ and $m = 6$, which correspond to a feed gain of 11.4dB and an aperture efficiency of about 80%. With these values, a lens of 5λ radius gives a Gaussian pattern of about 29dB gain.

IV. NUMERICAL VALIDATION

A. RAY-TRACING

A ray-tracing algorithm, has been developed in order to carry out a numerical validation of the presented work [28]. For a given $n(\rho)$, the ray-tracer kernel derives the ray-paths inside the inhomogeneous lens by solving the ray-equation, and the Poynting vector at the lens aperture by solving the energy transport equation, which expresses the conservation of the energy in a ray-tube. Fig. 6 shows the rays traced inside the GRIN lens, with evidence of spill-over and captured rays that contributes to the definition of the spill-over efficiency.

Fig. 7 shows the normalized Poynting vector at the output lens interface for different values of d/a, assuming $m = 12$ for the primary feed pattern in (10). The results are compared with the analytical form in (23).

B. FULL-WAVE ANALYSIS

A full wave analysis has been carried out by using the CST Microwave Studio Suite simulator. The model is composed by a point source embedded in a cylindrical lens. The lens is characterized by a radius of 5λ and by a radially varying refractive index $n(\rho)$. The latter is given by (14) once d/a and n_0 has been fixed. The point source feed has been modeled as an array of two Huygens's sources in a dipole-loop configuration that achieves approximately a $U(\theta) = \cos^3(\theta)$ pattern. At the lower interface, the lens is shielded by a metallic ground plane. The directivity of the antenna is calculated

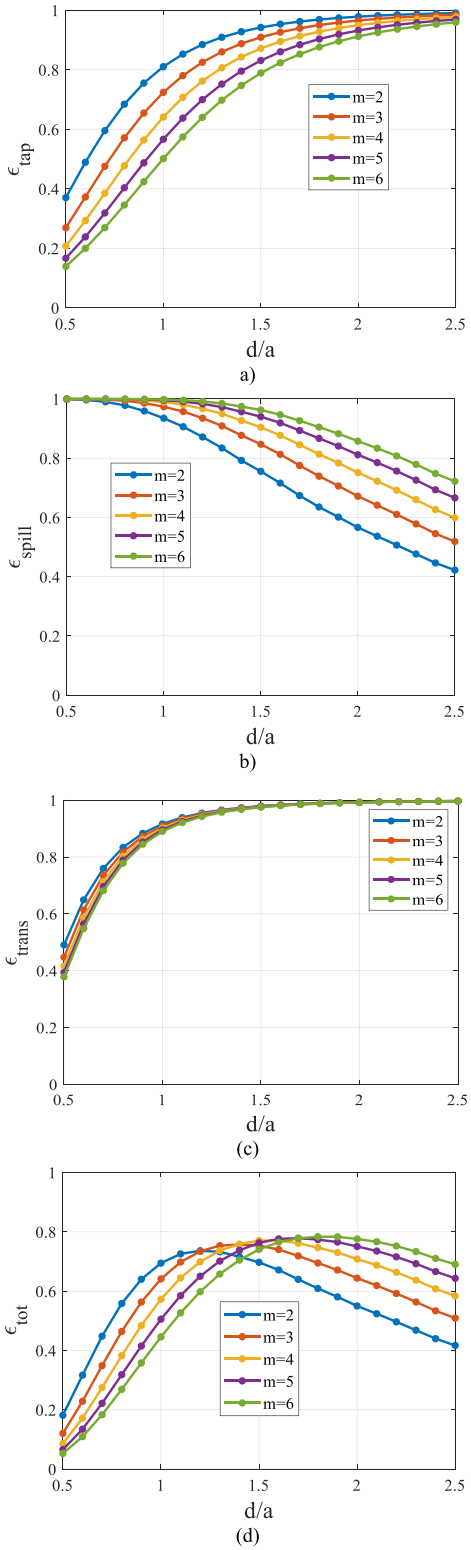

FIGURE 5. Individual and total efficiency contributions -as a function of *d/a* for different exponent in $U(\theta) = \cos^m \theta$ feed pattern. (a) tapering efficiency (ε_{tap}); (b) spill-over efficiency (ε_{spill}); (c) transmission efficiency(ε_{trans}); (d) total efficiency(ε_{tot}).

by the full wave analysis by dividing the power density for the radiated power obtained integrating the normalized radiation pattern and next dividing by the area of the interface.

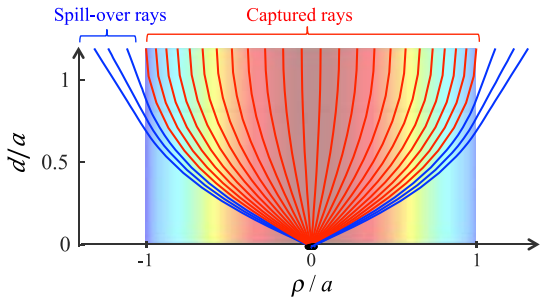

FIGURE 6. Ray-paths from ray-tracer: spill-over and captured rays.

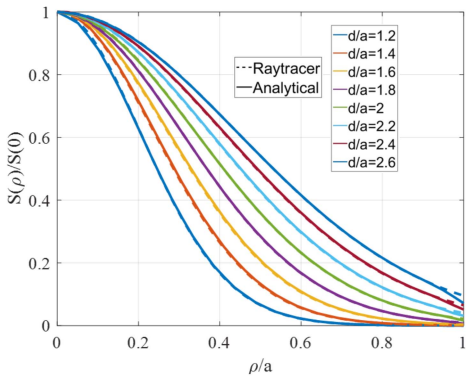

FIGURE 7. Normalized power density S(ρ)/S(0) as a function of ρ/a for primary feed pattern with $m = 12$. Comparison between the analytical solution (solid lines) and the results from ray-tracer (dashed).

TABLE 1. Comparison between CST and closed form formula.

d/a	n_0	ε_{tap} (30)	ε_{spill} (31)	ε_{trans} (28)	ε_{tot}	ε_{tot} (CST)	Gain (25)	Gain (CST)
1	2.5	0.72	0.97	0.9	0.64	0.56	28	27.4
1.2	2	0.82	0.94	0.95	0.73	0.79	28.6	28.9
1.4	1.7	0.89	0.88	0.97	0.76	0.81	28.8	29
1.6	1.5	0.93	0.81	0.98	0.74	0.81	28.6	29
1.8	1.4	0.95	0.74	0.99	0.7	0.77	28.4	28.8
2	1.3	0.97	0.67	0.99	0.64	0.72	28	28.5

Fig. 8(a) shows a comparison between the full-wave based total efficiency for a lens of radius 5λ and different value of *d/a*; these values are compared with the efficiency calculated through the closed form (30)-(31). Fig. 8(b)-(f) shows the directivity radiation pattern for various cases; insets in the various pictures show the snapshot of the real part of the electric field propagating inside the lens.

Table 1 summarizes the closed form formulas with the one obtained by CST for the cases shows in Fig. 8a. It is seen that our formulas underestimate the full-wave values of efficiency of few percent. This is probably due to the fact that the polarization as well as back radiation from the feed is not described properly in our formulas.

V. EXAMPLES

A. GRIN BY HOLES IN DIELECTRIC HOST MEDIUM

The GRIN lens may be realized by varying the hole density in a dielectric host medium, practically realizing or

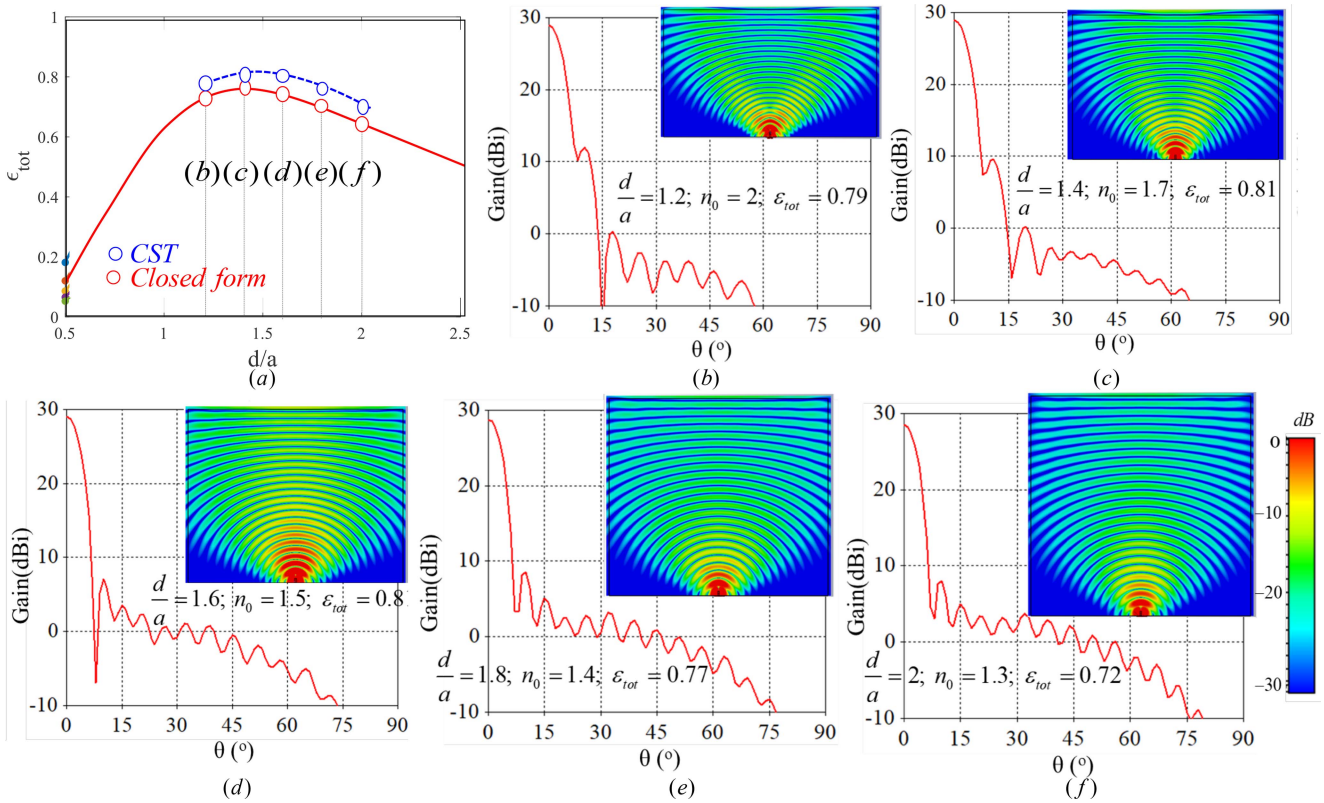

FIGURE 8. (a) Comparison between full-wave total efficiency (CST) and efficiency calculated by the closed form in (30)-(31); (b)-(f) gain patterns achieved for a lens of radius 5λ for different values of d/a. (b) $d/a = 1$, (c) $d/a = 1.2$, (d) $d/a = 1.4$, (e) $d/a = 1.6$, (f) $d/a = 1.8$; (f) $d/a = 2$. The insets present a snapshot of the real part of the in-plane transverse electric field. The feed is relevant to a doublet huyigens source with 9dB gain ($m = 3$).

by drilling a solid dielectric or by additive manufacturing. We consider here two examples, in which the dielectric host medium is Acrylonitrile Butadiene Styrene (ABS) and Teflon, characterized by a dielectric permittivity $\varepsilon_r = 2.7$, and $\varepsilon_r = 2.1$, respectively. The ABS is normally used in 3D printers. For both materials we will consider both square or circular holes, the first ones easier to be done by 3D printer and the second ones by drilling. Once one has fixed $n_0 = \varepsilon_r^{1/2}$ and the radius of the lens, the lens thickness d is derived from (15). If we fix $a = 3.12$ cm we obtain $d = 5.35$ cm and $d = 4.3$ cm for Teflon and ABS, respectively.

In order to synthesize the graded index by holes, the cylindrical lens has been subdivided in N cylindrical ideal concentric shells, with average radius centred at ρ_i with $i = 1, \ldots N$, each one with constant width $\delta = 2.4\text{mm} < \lambda/4$, (where λ is the free-space wavelength at 30GHz). Each shell has been filled by an entire number of holes (either square or circular) with cross-section areas s_i^2, constant in azimuth, like those shown in Fig. 9.

In each shell perimeter we can accommodate an integer number of holes equal to $N_i = [2\pi\rho_i/\delta]$, where [.] here denotes the integer part of the argument. This allows the cell containing a single hole to be almost square (see Fig. 10). The equivalent permittivity has been computed by averaging the full and empty volume permittivity, as

$$\varepsilon_i = \frac{V_{holes,i} + \varepsilon_r\left(V_{shell,i} - V_{holes,i}\right)}{V_{shell,i}} \tag{32}$$

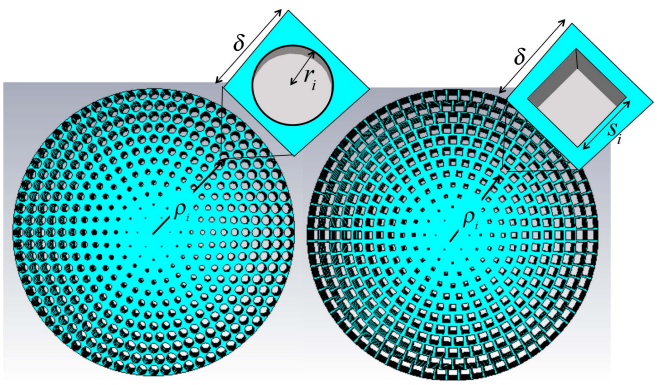

FIGURE 9. CAD models of the GRIN lens; (a) circular holes; (b) square holes.

In (32), $\varepsilon_i = n^2(\rho_i)$, is a sampling of the desired continuous refractive index $n(\rho)$ to be synthesized, defined in (14).

Furthermore, $V_{holes,i}$ is the empty volume associated to the ith shell, $V_{shell,i}$ is the volume of the i-th shell, and $\varepsilon_r = n_0^2$ is the relative permittivity of Teflon or ABS, respectively. The hole height has been fixed equal to the entire lens thickness d in order to preserve the longitudinal homogeneity. Thus, one has $V_{holes,i} = N_i s_i^2 d$ and $V_{shell,i} = 2\pi\rho_i\delta d$. Eq. (32) can be therefore inverted to find s_i^2

$$s_i^2 = \frac{2\pi\rho_i\delta(\varepsilon_i - \varepsilon_r)}{N_i(1 - \varepsilon_r)} \tag{33}$$

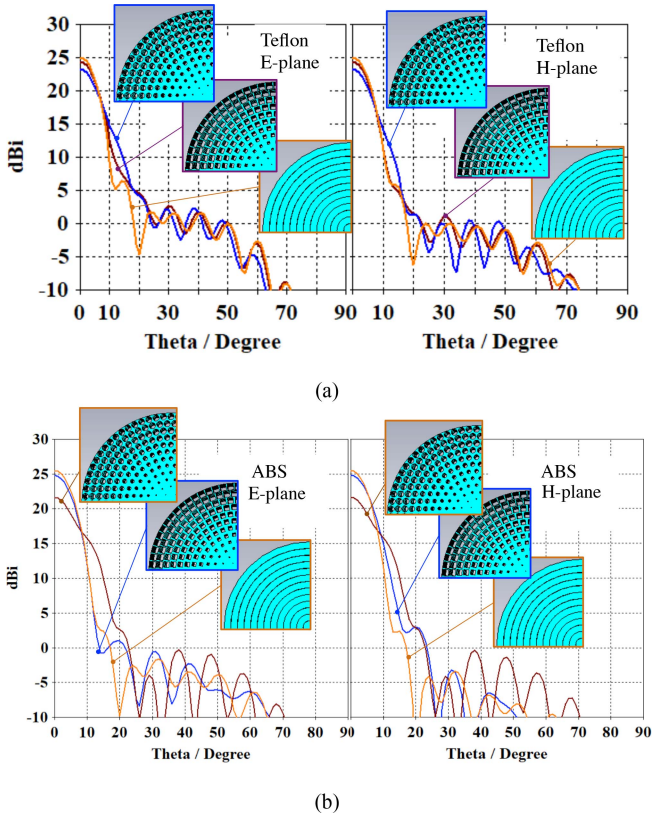

FIGURE 10. Gain patterns for the GRIN lens design with (a) $\varepsilon_r = 2.1$ (Teflon), d = 5,35, a = 3.12λ and (b) $\varepsilon_r = 2.1$ (Teflon), $d = 4.53\lambda$, a = 3.12λ, at a working frequency $f_0 = 30$ GHz, obtained by square holes, circular holes and homogeneous cylindrical shell, respectively. E-plane and H-plane are on the left hand side and right hand side, respectively.

In (33) s_i is either the side of the square holes or it is related to the radius of the circular holes through $S_i^2 = \pi r_i^2$ (see inset of Fig. 10). The adopted discretization and homogenization processes produce two kind of errors in the permittivity profile of the GRIN lens wrt the ideal one: i) a discretization error due to the approximation of a continuous profile with a step profile ii) a homogenization error due to the unavoidable approximation of N_i to an integer number. It is seen that the average discretization error for Teflon is 0.2% (ABS 0.4%), while the average homogenization error is 2.6% (4%) for circular holes and 2% (2.8%) for square holes. Therefore, the homogenization error is prevalent with respect to the discretization error and increases with the permittivity of the host medium. Therefore, the square-holes solution is preferable. This is confirmed by the numerical results of the next section.

B. NUMERICAL RESULTS

Full-wave CST simulations has been carried out for the lens described in the previous section ($a = 3, 12$ cm, d = 4.3 cm, with center frequency at 30 GHz). The lens has been fed in both ABS and Teflon case by a circular waveguide of radius 2.8 mm, filled by the pertinent dielectric, fed by a TE11 mode and integrated in the lens. The radiation intensity pattern of this open-ended waveguide when it radiates

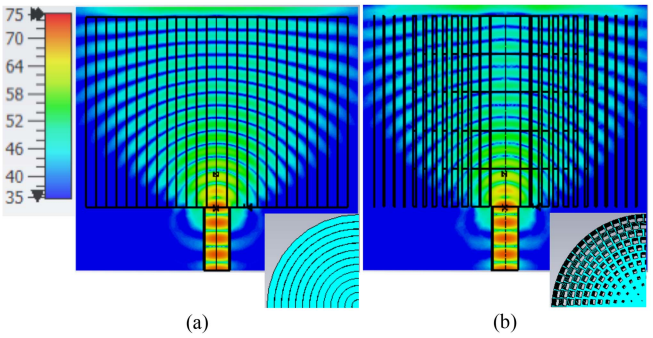

FIGURE 11. Snap-shoot of the real part of the E-plane Field distribution for the GRIN lens with $\varepsilon_r = 2.1$ (Teflon) at $f_0 = 30$ GHz. (a) cylindrical shells, (b) square holes.

into an infinite medium with the same relative permittivity approximates eq. (21) with $m = 3$ for both Teflon and ABS. Our formulas predict a total aperture efficiency of 70% for Teflon and 76% for ABS. Fig. 10 presents the gain- patterns in the E-plane and H-plane obtained by square holes, circular holes and homogeneous cylindrical shell, respectively. Fig. 10a and 10b are relevant to Teflon and ABS, respectively.

As expected, it is seen that the square-holes cases better fits the reference case of homogeneous cylindrical shell. For the case of Teflon, the maximum directivity for homogeneous cylindrical shell is given by 25 dB (aperture efficiency equal to 80%) against 24.3dB for square-holes (70%) and 23.2dB (55%) for circular holes. For the case of ABS, the aperture efficiency is equal to 85% against 80% for square-holes and 45% for circular holes, in line with our prediction. Furthermore, the radiation patterns for the square holes are in better agreement with the reference ideal one. Furthermore the Teflon case shows a better symmetry in the two planes.

A snapshot of the real part of the electric field inside the Teflon lens is presented in Fig. 11(a) for cylindrical-shell lens and in Fig. 11a for square-holes lens. It can be clearly seen that the spherical wavefront delivered by the waveguide is gradually transformed in planar phase fronts at the lens aperture. Equally well for both the cylindrical shells and for the square-holes.

A further possible application of the proposed formulation is to consider a model of a shaped GRIN lens where the metallic wall profile follows the extreme ray-path. We will refer to it as "cup-lens". The external-wall profile of the cup-lens is designed following the mathematical expression in (17) with $\theta = \theta_{max}$. Two cases have been considered where the walls are covered or not by a perfectly electric conductor. Fig. 12a and 12b show the E-field inside the lens without and with external metallization, respectively. The far field directivity pattern is indeed shown in Fig. 12c and 12d, respectively. It is seen that the two principal-plane cuts exhibit a good symmetry in the main lobe, especially for metallized walls, as it occurs in scalar horns. The cross-polar components in these cases are below −35 dB with respect to the maximum of the co-polar components, as typically

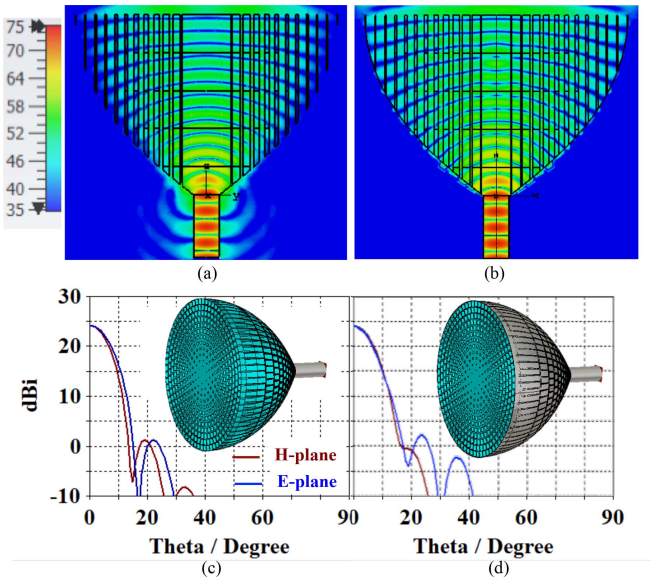

FIGURE 12. Snap-shoot of the real part of the E-plane field distribution for the GRIN cup-lens at $f_0 = 30$ GHz realized by square-holes. (a) case without metallic walls; (b) with metal walls. Directivity pattern in the E-plane and H-plane for the structure without metallic walls (c) and with metallic walls (d). The level of the cross-polar components are outside the represented scale.

occurs in scalar horns. Also, the pattern profile approaches a Gaussian shape in all planes.

VI. CONCLUSION

Design formulas for a new compact GRIN lens with integrated feed have been derived. The exact expression of the refractive index profile has been obtained by applying the inverse truncated Abel transform to a ray-path congruence equation given by GO. The exact relationship between the lens geometrical parameters (d/a) and the maximum value of the refractive index (n_0) allows a simple design of the antenna. The Poynting vector at the lens aperture, assuming a $\cos^m\theta$-type feeder, has been achieved by applying the conservation of energy in ray-tubes. The latter can be approximated with a Gaussian profile and this allows for achieving aperture efficiency in closed form. The resulting total efficiency may be designed till a value of 80%. The closed form results have been successfully validated with an in-house ray-tracing algorithm, based on GO, and by full-wave simulations. Finally, we have presented practical design of GRIN lenses by using holes in a Teflon or ABS host media, including a case of a cup-horn designed by the analytical profile of the extreme ray-path. This opens the possibility to simply design a new type of all-dielectric scalar (Gaussian) horn, which constitutes a reduced-volume alternative to corrugated horns [26] or to profiled conical horn with dielectric loading [27] and will be the subject of a future dedicated work.

ACKNOWLEDGMENT

The authors wish to thank Bruno Biscontini and Alejandro Murillo of Huawei, Munich, for useful discussion on this subject.

REFERENCES

[1] H. F. Ma, B. G. Cai, T. X. Zhang, Y. Yang, W. X. Jiang, and T. J. Cui, "Three-dimensional gradient-index materials and their applications in microwave lens antennas," *IEEE Trans. Antennas Propag.*, vol. 61, no. 5, pp. 2561–2569, May 2013.

[2] H.-X. Xu, G.-M. Wang, Z. Tao, and T. Cui, "An octave-bandwidth half Maxwell fish-eye lens antenna using three-dimensional gradient-index fractal metamaterials," *IEEE Trans. Antennas Propag.*, vol. 62, no. 9, pp. 4823–4828, Sep. 2014.

[3] D. Schurig, "An aberration-free lens with zero F-number," *New J. Phys.*, vol. 10, Nov. 2008, Art. no. 115034.

[4] N. I. Landy, N. Kundtz, and D. R. Smith, "Designing three-dimensional transformation optical media using quasiconformal coordinate transformations," *Phys. Rev. Lett.*, vol. 105, Nov. 2010, Art. no. 193902.

[5] C. Mateo-Segura, A. Dyke, H. Dyke, S. Haq, and Y. Hao, "Flatluneburg lens via transformation optics for directive antenna applications," *IEEE Trans. Antennas Propag.*, vol. 62, no. 4, pp. 1945–1953, Apr. 2014.

[6] U. Leonhardt, "Optical conformal mapping," *Science*, vol. 312, no. 5781, pp. 1777–1780, 2006. [Online]. Available: http://science.sciencemag.org/content/312/5781/1777

[7] J. B. Pendry, D. Schurig, and D. R. Smith, "Controlling electromagnetic fields," *Science*, vol. 312, no. 5781, pp. 1780–1782, 2006. [Online]. Available: http://science.sciencemag.org/content/312/5781/1780

[8] S. Jain, M. Abdel-Mageed, and R. Mittra, "Flat-lens design using field transformation and its comparison with those based on transformation optics and ray optics," *IEEE Antennas Wireless Propag. Lett.*, vol. 12, pp. 777–780, 2013.

[9] B. Q. Lu, Z. H. Jiang, and D. H. Werner, "Far-zone focusing lenses designed by complex coordinate transformations," *IEEE Antennas Wireless Propag. Lett.*, vol. 13, pp. 1779–1782, 2014, doi: 10.1109/LAWP.2014.2356173.

[10] D. E. Brocker, J. P. Turpin, P. L. Werner, and D. H. Werner, "Optimization of gradient index lenses using quasi-conformal contour transformations," *IEEE Antennas Wireless Propag. Lett.*, vol. 13, pp. 1787–1791, 2014.

[11] R. K. Luneburg, *Propagation of Electromagnetic Waves*. New York, NY, NY, USA: New York Univ., 1948.

[12] M. Kline, "An asymptotic solution of Maxwell's equations," *Commun. Pure Appl. Math.*, vol. 4, nos. 2–3, pp. 225–263, 1951.

[13] M. Born and E. Wolf, *Principles of Optics*. Cambridge, U.K.: Cambridge Univ. Press, 1999.

[14] L. B. Felsen and N. Marcuvitz, "Radiation and scattering of waves," in *Electromagnetic Wave Theory*. Piscataway, NJ, USA: IEEE Press, 1994.

[15] E. T. Kornhauser and A. D. Yaghjian, "Modal solution of a point source in a strongly focusing medium," *Radio Sci.*, vol. 2, no. 3, pp. 299–310, Mar. 1967.

[16] Y. Silberberg and U. Levy, "Modal treatment of an optical fiber with a modified hyperbolic secant index distribution," *J. Opt. Soc. America*, vol. 69, no. 7, pp. 960–963, 1979.

[17] S. Zhang, R. K. Arya, S. Pandey, Y. Vardaxoglou, W. Whittow and R. Mittra, "3D-printed planar graded index lenses," *IET Microw. Antennas Propag.*, vol. 10, no. 13, pp. 1411–1419, 2016.

[18] X. Chen, H. F. Ma, X. Y. Zou, W. X. Jiang, and T. J. Cui, "Three-dimensional broadband and high-directivity lens antenna made of meta- materials," *J. Appl. Phys.*, vol. 110, no. 4, 2011, Art. no. 044904.

[19] N. Zhang, W. X. Jiang, H. F. Ma, W. X. Tang, and T. J. Cui, "Compact high-performance lens antenna based on impedance-matching gradient-index metamaterials," *IEEE Trans. Antennas Propag.*, vol. 67, no. 2, pp. 1323–1328, Feb. 2019.

[20] S. Zhang, R. K. Arya, W. G. Whittow, D. Cadman, R. Mittra, and J. Vardaxoglou, "Ultra-wideband flat metamaterial GRIN lenses assisted with additive manufacturing technique," *IEEE Trans. Antennas Propag.*, early access, Dec. 21, 2020, doi: 10.1109/TAP.2020.3044586.

[21] J. Budhu and Y. Ramhat-Samii, "A Novel and systematic approach to inhomogeneous dielectric lens design based on curved ray geometrical optics and particle swarm optimization," *IEEE Trans. Antennas Propag.*, vol. 67, no. 6, pp. 3657–3669, Jun. 2019.

[22] C. A. Balanis, *Antenna Theory: Analysis and Design*, 2nd ed. New York, NY, USA: Wiley, Inc., 1997.

[23] I. S. Gradshteyn and I. M. Ryzhik, *Table of Integrals, Series and Products*, 2nd ed. San Diego, CA, USA: Academic, 1980.
[24] P. D. Potter, "A new horn antenna with suppressed sidelobes and equal beamwidth," *Microwave J.*, vol. 6, pp. 71–78, Jun. 1963.
[25] H. M. Pickett, J. C. Hardy, and J. Farhoomand, "Characterization of a dual-mode horn for submillimeter wavelengths," *IEEE Trans. Microw. Theory Techn.*, vol. 32, no. 8, pp. 936–937, Aug. 1984.
[26] P. J. B. Clarricoats and A. D. Oliver, *Corrugated Horns for Microwave Antennas* (Electromagnetic Waves). London, U.K.: Inst. Electr. Eng., 1984.
[27] S. Zhang, D. Cadman, and J. Y. C. Vardaxoglou, "Additively manufactured profiled conical horn antenna with dielectric loading," *IEEE Antennas Wireless Propag. Lett.*, vol. 17, no. 11, pp. 2128–2132, Nov. 2018.
[28] F. Maggiorelli, A. Paraskevopoulos, A. Albani, and S. Maci, "Raytracing in dielectric inhomogeneous lenses," in *Proc. 14th Eur. Conf. Antennas Propag.*, Mar. 2020, pp. 1–3.

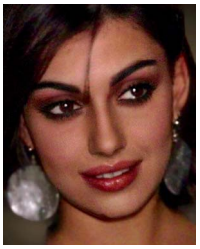

FRANCESCA MAGGIORELLI received the bachelor's degree in telecommunication engineering from the University of Siena, Siena, Italy, in 2009, the master's degree in biomedical engineering from the University of Pisa, Pisa, Italy, in 2015, and the Ph.D. degree from the University of Siena in 2018. During her Ph.D. studies, she worked in collaboration with the National Institute of Nuclear Physics (INFN–Pisa Division, Italy) and the IMAGO7 Foundation, Pisa, focusing her research activity on the design and development of RF double tuned coils for magnetic resonance imaging at ultrahigh field. Her current research interests inhomogeneous lenses analysis and design.

ANASTASIOS PARASKEVOPOULOS was born in Athens, Greece, in 1988. He received the Diploma degree in electrical and computer engineering from the Democritus University of Thrace, Xanthi, Greece, in 2012, and the Ph.D. degree from Loughborough University, U.K., for his research entitled "Body-Centric Wireless Communications: Wearable Antennas, Channel Modeling, and Near-Field Antenna Measurements" in 2017. From 2016 to 2019, he worked as a Research Assistant with the Department of Digital Systems, University of Piraeus, Greece, participating in European Union's Horizon 2020 projects. He is currently with the Electromagnetics Group, University of Siena. His research interests include the design of artificially engineered materials with a focus on gradient index lenses for antenna applications. He is also involved in antenna characterization through near-field and far-field measurements in the anechoic chamber.

J. (YIANNIS) C. VARDAXOGLOU (Fellow, IEEE) received the B.Sc. degree in mathematical physics and the Ph.D. degree in electronics from the University of Kent, U.K., in 1982 and 1985, respectively.

He joined Loughborough University as a Lecturer in 1988, was promoted to Senior Lecturer in 1992, and has been a Professor of wireless communications since 1998, where he served as the Dean of the School of Electronic, Electrical and Systems Engineering from 2006 to 2012. He is a guest visiting Professor with the University of Siena since 2020. He established the 32-year-old Wireless (WiCR) Group, Loughborough University and Communications Research founded the Centre for Mobile Communications Research. He is the Director of SYMETA Research Centre, funded by an EPSRC Grand Challenge Award, researching a wide-ranging topics applicable to cutting-edge wireless communications technology. SYMETA collaborates with many internationally leading companies and universities. He has served as a consultant to various industries, holds six patents and is the Founder/Technical Director of Antrum Ltd. He has attracted research funding from industry and has been awarded 20 EPSRC research grants. He has published over 400 refereed journals and conference proceeding papers (with over 8900 citations) and has written a seminal book on frequency selective surfaces. His current research focuses primarily on metamaterial structures, additive manufacturing (3-D printing) for RF/micro/mm wave engineering. He was awarded a prestigious EPSRC Grand Challenge £5M (FEC) Award: "Synthesizing 3-D Metamaterials for RF, Microwave, and THz Applications." He was the Chairman of the Executive Committee of the IET's Antennas and Propagation Professional Network in the U.K. and chaired the IEEE's Distinguish Lecturer Program of the Antennas and Propagation Society for five years. He founded the Loughborough Antennas and Propagation Conference, which has been running since 2005. He has chaired numerous IEE/IET events and has served on the Steering Committee of the European Conference on Antennas and Propagation, EuCAP. He was the General Chair of EuCAP'07. He is a Fellow of the Royal Academy of Engineers.

MATTEO ALBANI (Fellow, IEEE) received the Laurea degree in electronic engineering and the Ph.D. degree in telecommunications engineering from the University of Florence, Florence, Italy, in 1994 and 1999, respectively.

From 2001 to 2005, he was an Assistant Professor with the University of Messina, Messina, Italy. He is currently an Associate Professor with the Information Engineering and Mathematics Department, University of Siena, Siena, Italy, where he is also the Director of the Applied Electromagnetics Laboratory. He has coauthored more than 80 journal articles and book chapters, more than 200 conference papers, and five patents. His research interests are in the areas of high-frequency methods for electromagnetic scattering and propagation, numerical methods for array antennas, antenna analysis and design, metamaterials, and metasurfaces.

Dr. Albani received the "G. Barzilai" Young Researcher Best Paper Award at the XIV RiNEM, Ancona, Italy, in 2002, and the URSI Commission B Young Scientist Award at the 2004 URSI EMTS, Pisa, Italy. He was a co-author with and an advisor to the winners of the Best Paper Award at the First European AMTA Symposium in 2006, Munich, Germany, and of the Third Prize Young Scientist Best Paper Award at the 2010 URSI EMTS, Berlin, Germany. With his coauthors, he also received the Antenna Theory Best Paper Award at the EuCAP 2014, Hague, The Netherlands, and the Antenna Theory Best Paper Award at the EuCAP 2018, London, U.K. He is a member of EurAAP and URSI.

STEFANO MACI (Fellow, IEEE) received the Laurea degree (*cum laude*) from the University of Florence in 1987.

Since 1997, he has been a Professor with the University of Siena. From 2004 to 2007, he was a WP Leader with the Antenna Center of Excellence (ACE, FP6-EU) and a International Coordinator of a 24-institution consortium of a Marie Curie Action (FP6) from 2007 to 2010. Since 2010, he has been a Principal Investigator of six cooperative projects financed by European Space Agency. In 2004, he was the Founder of the European School of Antennas (ESoA), a post graduate school that presently comprises 34 courses on Antennas, Propagation, Electromagnetic Theory, and Computational Electromagnetics and 150 teachers coming from 15 countries. Since 2004, he has been the Director of ESoA. From 2008 to 2015, he was the Director of the Ph.D. Program in Information Engineering and Mathematics, University of Siena, and from 2013 to 2015, he was a member of the first National Italian Committee for Qualification to Professor. He is the Director of the consortium FORESEEN, currently involving 48 European Institutions. He was the Principal Investigator of the Future Emerging Technology Project "Nanoarchitectronics" of the 8th EU Framework program, and currently a Principal Investigator of the EU Program "Metamask." His research activity is documented in 170 papers published in international journals, (among which 100 on IEEE journals), ten book chapters, and about 450 papers in proceedings of international conferences. The papers he coauthored have been cited about 7800 times (source: Google Scholar). His research interests include high-frequency and beam representation methods, computational electromagnetics, large phased arrays, planar ntennas, reflector antennas and feeds, metamaterials, and metasurfaces.

Prof. Maci was a recipient of the EurAAP Award in 2014, the IEEE Schelkunoff Transaction Prize in 2016, the Chen-To Tai Distinguished Educator Award in 2016, and the URSI Dellinger Gold Medal in 2020. He has been a TPC Chair of the METAMATERIAL 2020 conference and designed Chairperson of EuCAP 2022. In the last ten years, he has been invited 25 times as key-note speaker in international conferences. In 2000, he was a member of the Technical Advisory Board of 12 international conferences and the Review Board of six International Journals. He has been a Former Member of the AdCom of IEEE Antennas and Propagation Society (AP-S), an Associate Editor of IEEE TRANSACTIONS ON ANTENNAS AND PROPAGATION, the Chair of the Award Committee of IEEE AP-S, and a member of the Board of Directors of the European Association on Antennas and Propagation (EurAAP). He has been a Former Member of the Antennas and Propagation Executive Board of the Institution of Engineering and Technology, U.K. He was a Co-Founder of two Spin-off Companies. He is a Distinguished Lecturer of IEEE AP-S, EuRAAP, and ambassador program.